A Self-Calibrating Temperature Independent Model of a Bi-Axial Piezoelectric MEMS Tilt Sensor

Paul M. Moubarak[a], Danielle A. Barsky[a], Pinhas Ben-Tzvi[a], Mona Zaghloul[b]
[a] Robotics and Mechatronics Lab, Department of Mechanical and Aerospace Engineering, The George Washington University, Washington, DC 20052, USA
[b] Department of Electrical and Computer Engineering, The George Washington University, Washington, DC 20052, USA

ABSTRACT

The dual-axis piezoelectric tilt measurement device presented in this paper is modeled using a proposed methodology that generates a self-calibrating representation of the sensor's output around two axes. Typically, when a piezo-based sensor is developed, its output is modeled as a direct function of its geometric, electro-mechanical and piezoelectric properties. This means that an accurate representation of the sensor's output requires an accurate knowledge of its characteristics. In piezoelectric MEMS applications however, such information is either not available, or is provided in the form of approximate values which are susceptible to external stimuli. The method proposed in this paper models the direct piezoelectric effect as a function of genetic data provided *a priori* about the operation of a piezo-system. The resulting model is shown to be independent of any system-specific characteristics or any external stimuli. The impact that these parameters exhibit on the output of the sensor is carried implicitly by the genetic data which is generated through calibration. The validity of the proposed model is demonstrated through simulations performed on a new piezoelectric device for dual-axis tilt measurement. These results show a considerable accuracy under variations in the operating conditions, such as temperature.

Keywords: Tilt sensor, MEMS, direct piezoelectric effect, self-calibrating model, dual-axis

1. INTRODUCTION

The direct piezoelectric effect is a phenomenon exhibited by crystalline materials, such as quartz and ceramics, where the application of a mechanical stress forces a re-alignment of the electric dipoles which generates an electrical charge across the faces of the crystal. This phenomenon can be exploited in many engineering applications, most notably in sensor applications where the stress-inducing capability of a stimulus, such as pressure[1] or acceleration[2], is converted into a proportional measurable metric, namely an electrical voltage.

From a mathematical perspective, modeling the direct effect of piezoelectricity is typically accomplished with constitutive equations which correlate the stress tensor T to the electrostatic field E through the piezoelectric coefficient matrix d and the permittivity matrix ε. This means that an accurate representation of the behavior of a piezo-mechanical system requires a complete knowledge of its electro-mechanical and piezoelectric properties. The drawback of this approach however is that the coefficients of matrix d and ε are approximate statistical values that are further affected by external stimuli, such as temperature[3 – 6], or by the operating conditions of the piezo-system, such as fatigue[7], crystal aging[8,9] and magnetically-induced depolarization[10]. This makes the resulting model vulnerable to unpredictable, unstable or time-varying parameters.

The compensation for this vulnerability is often done mathematically, by modeling the influence of each stimulus separately and adding its contribution to the initial constitutive equations making them heavily non-linear[11,12]. In this paper, we propose a new modeling approach for the direct piezoelectric effect which results in a self-calibrating model[13]. By self-calibration, we mean that the mathematical model does not depend explicitly on the geometric, structural and piezoelectric properties of the system. Instead, this information is carried implicitly by genetic data generated via calibration, and provided *a priori* about the operation of the system.

Although such modeling approach cannot be *currently* proven to being generalizable, its significance on system-to-system basis is highly desirable, especially for applications where the operating conditions of the piezo-system vary over time. As such, in this paper, a new piezoelectric tilt-sensor will be first presented, and its voltage output for dual-axis

Micro- and Nanotechnology Sensors, Systems, and Applications IV, edited by Thomas George, M. Saif Islam, Achyut Dutta, Proc. of SPIE Vol. 8373, 83732L
 · doi: 10.1117/12.918419

sensing applications will be modeled using the proposed self-calibrating approach. The ensuing mathematical derivation will be further validated via simulation results under varying thermal conditions.

2. DUAL-AXIS PIEZOELECTRIC TILT SENSOR

The proposed piezoelectric tilt sensor consists of a silicon substrate with a fixed-fixed 900 µm platinum beam suspended on the substrate, and carrying a proof mass in the center as illustrated schematically in Fig. 1. (Beam width: 20 µm). Under gravitational loading, the deflection of the beam – caused by the weight of the proof mass – generates a stress profile that peaks at the top surface of the beam near the anchors. This profile changes as a function of the roll and pitch angles of the sensor, since the components of the gravitational force causing the deflection represent a direct trigonometric function of these two angles.

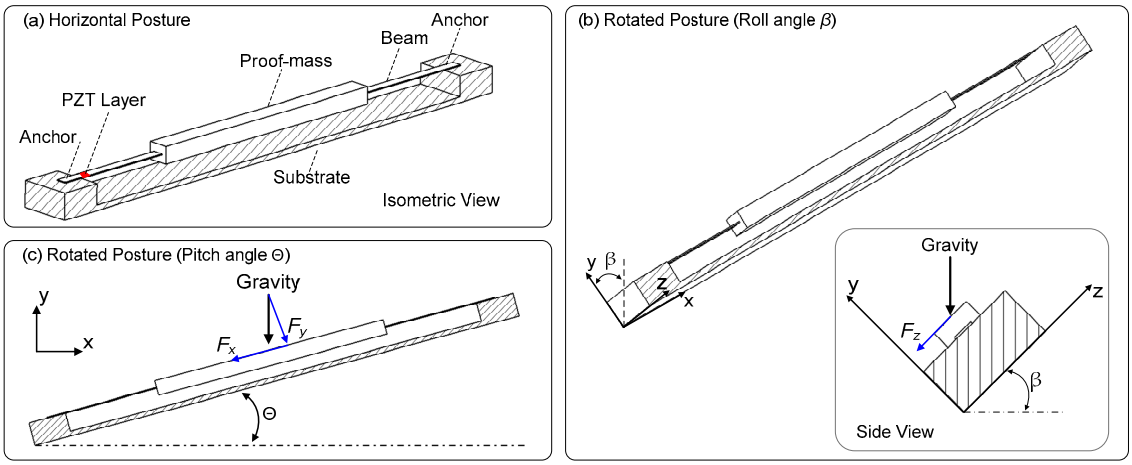

Figure 1. (a) Isometric schematic of the proposed piezoelectric tilt sensor, (b) Roll posture (β), (c) Pitch posture (θ)

This means that a piezoelectric layer of Lead Zirconate Titanate (PZT) deposited on the top surface of the beam where the peak stress occurs, converts the mechanical stress into a measurable voltage following the direct piezoelectric effect. Similar to the stress profile, such voltage is a function of the roll and pitch angles of the sensor as illustrated in the two simulation results provided in Fig. 2. In these simulations, it is shown that the voltage output of the PZT layer varies proportionally with the single-axis pitch and roll inclination of the sensor, where the two profiles start from the same value corresponding to the horizontal posture of the sensor, and descend smoothly towards zero at 90° following two distinct slope profiles.

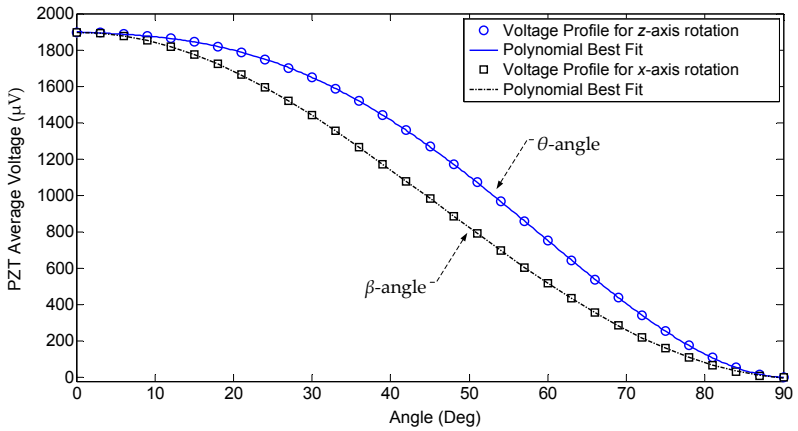

Figure 2. PZT voltage output profile for a single-axis roll (β) and pitch (θ) inclination

3. SELF-CALIBRATING MODEL DERIVATION

Modeling the dual-axis behavior of the tilt sensor in Fig. 1 where none of the angles is set at zero requires a thorough derivation of the constitutive equations. In the proposed self-calibrating approach, we show that the dual-axis sensor output can be modeled as a function of the single-axis behavior (Fig. 2) which represents the genetic data for this sensor.

The initial process in this derivation consists of curve-fitting the genetic data with a polynomial of order *n* that best approximates the data. These polynomials can be written as

$$V_{\beta,0} = \sum_{p=0}^{n} a_p \beta^{n-p}, \qquad V_{0,\theta} = \sum_{p=0}^{n} b_p \theta^{n-p} \tag{1}$$

where $V_{\beta,0}$ (μV) represents the PZT voltage output for any angle β (Deg) at $\theta = 0°$, $V_{0,\theta}$ (μV) the PZT voltage output for any angle θ (Deg) at $\beta = 0°$, and a and b the polynomial coefficients. Furthermore, the decomposition of the gravitational force $F = Mg$ generated by the proof mass M into its three-dimensional components in the reference Cartesian frame *xyz*, where *z* defines the gravitational direction

$$F_x = F\cos(\beta)\sin(\theta) \qquad F_y = F\cos(\beta)\cos(\theta) \qquad F_z = F\sin(\beta) \tag{2}$$

enables the expansion of the components of the stress tensor $T = \begin{bmatrix} T_1 & T_2 & T_3 & T_4 & T_5 & T_6 \end{bmatrix}^T$ as follows

$$T_1 = \frac{a_{11} F\cos(\beta)\sin(\Theta)}{A_x} + \frac{a_{12} F\cos(\beta)\cos(\Theta) x_p y_p}{I_z} + \frac{a_{13} F\sin(\beta) x_p z_p}{I_y} \tag{3}$$

$$T_2 = \frac{a_{21} F\cos(\beta)\cos(\theta)}{A_y} \tag{4}$$

$$T_3 = \frac{a_{31} F\sin(\beta)}{A_z} \tag{5}$$

$$T_4 = \frac{a_{41} F\cos(\beta)\cos(\theta) Q_x}{I_x t_x} \tag{6}$$

$$T_5 = \frac{a_{51} F\sin(\beta) Q_y}{I_y t_y} \tag{7}$$

$$T_6 = \frac{a_{61} F\cos(\beta)\sin(\theta) Q_z}{I_z t_z} \tag{8}$$

where, in (3) to (8), A_x, A_y, A_z define the area of the beam's cross-section orthogonal to the *x*, *y* and *z* axes, respectively, I_x, I_y, I_z the area moment of inertia of the beam's cross-section around the *x, y* and *z* axes, respectively, Q_x, Q_y, Q_z the first moment of area of the beam's cross-section around the *x, y* and *z* axes, respectively, t_x, t_y, t_z the thickness of the cross-section perpendicular to the corresponding shear and measured with respect to the beam's neutral fiber, and x_p, y_p, z_p the coordinates of the points of interest on the beam where the calculation of the stress tensor is being performed. Furthermore, a_{ij} are constant coefficients appended to the stress element T_i to account for the sign contribution of each element, and to aggregate all numerical constants pertinent to each expression.

The expansion of the stress tensor elements shows that T is a direct function of β and θ. This means that the polarization vector D and the electrostatic field E are also functions of β and θ based on the constitutive equations

$$D(\beta,\Theta) = d\ T(\beta,\Theta), \qquad E(\beta,\Theta) = \varepsilon^{-1} D(\beta,\Theta) \tag{9}$$

In (9), the expansion of the vector components of $E(\beta,\theta)$ generates trigonometric expressions for E_1, E_2, E_3 in terms of β and θ as follows

$$E_1 = k_1 \sin(\beta), \qquad E_2 = k_2 \cos(\beta)\cos(\theta)$$
$$E_3 = k_3 \cos(\beta)\sin(\theta) + k_4 \cos(\beta)\cos(\theta) + k_5 \sin(\beta) + k_6 \cos(\beta)\cos(\theta) + k_7 \sin(\beta) \tag{10}$$

where in (10), all coefficients and terms that are not an explicit function of β and θ are lumped into coefficients k_i. With this nomenclature, the voltage $V_{\beta,\theta}$ across the faces of the beam can be written as a line integral of the electrostatic field $E(\beta,\theta)$ as

$$V_{\beta,\Theta} = \int_C E(\beta,\Theta)\cdot dl = E\cdot\hat{n}\,\|\,\Delta L\,\| \tag{11}$$

where $\hat{n}$ denotes a unit vector in the ΔL direction, and $\|\Delta L\|$ the magnitude of vector $\Delta l = (w+\delta w)\hat{x} + (t+\delta t)\hat{y} + (b+\delta b)\hat{z}$ with w,t,b denoting the width, thickness and base length of the PZT layer, respectively, and $\delta w, \delta t, \delta b$ their respective variations under tensile/compressive loading. Furthermore, if one writes $E = \| E \|\hat{e}$, where $\hat{e}$ is an arbitrary unit vector in the direction of vector E, then (11) can be re-written as $V_{\beta,\theta} = \| E \|\,\|\Delta L\|\cos(\hat{e},\hat{n}) = \lambda \| E \|$ where $\lambda = \|\Delta L\|\cos(\hat{e},\hat{n})$ represents a geometric scalar that is an implicit function of β,θ. The squared expression of $V_{\beta,\theta}$ can then be expanded with E as in (10) into the form

$$\begin{aligned} V^2_{\beta,\theta} &= K_1\sin^2(\beta) + K_2\cos^2(\beta)\cos^2(\theta) + K_3\cos^2(\beta)\sin^2(\theta) + K_4\cos^2(\beta)\cos^2(\theta) + K_5\sin^2(\beta) + K_6\cos^2(\beta)\cos^2(\theta) \\ &+ K_7\sin^2(\beta) + K_8\cos^2(\beta)\sin(\theta)\cos(\theta) + K_9\sin(\beta)\cos(\beta)\sin(\theta) + K_{10}\cos^2(\beta)\sin(\theta)\cos(\theta) + K_{11}\sin(\beta)\cos(\beta)\sin(\theta) \\ &+ K_{12}\sin(\beta)\cos(\beta)\cos(\theta) + K_{13}\cos^2(\beta)\cos^2(\theta) + K_{14}\sin(\beta)\cos(\beta)\cos(\theta) + K_{15}\sin(\beta)\cos(\beta)\cos(\theta) \\ &+ K_{16}\sin^2(\beta) + K_{17}\sin(\beta)\cos(\beta)\cos(\theta) \end{aligned} \tag{12}$$

where $K_{1-7} = \lambda^2 \prod_{i=1}^{7} k_i k_i$ and $K_{8-17} = 2\lambda^2 \prod_{i=3}^{6}\prod_{j=i+1}^{7} k_i k_j$. From (12), an expression for $V_{\beta,0}$ can be derived by setting $\theta = 0°$

$$\begin{aligned} V^2_{\beta,0} &= K_1\sin^2(\beta) + K_2\cos^2(\beta) + K_4\cos^2(\beta) + K_5\sin^2(\beta) + K_6\cos^2(\beta) + K_7\sin^2(\beta) \\ &+ K_{12}\sin(\beta)\cos(\beta) + K_{13}\cos^2(\beta) + K_{14}\sin(\beta)\cos(\beta) + K_{15}\sin(\beta)\cos(\beta) + K_{16}\sin^2(\beta) + K_{17}\sin(\beta)\cos(\beta) \end{aligned} \tag{13}$$

Similarly, an expression for $V_{0,\theta}$ can be derived by setting $\beta = 0°$ in (12)

$$V^2_{0,\theta} = K_2\cos^2(\theta) + K_3\sin^2(\theta) + K_4\cos^2(\theta) + K_6\cos^2(\theta) + K_8\sin(\theta)\cos(\theta) + K_{10}\sin(\theta)\cos(\theta) + K_{13}\cos^2(\theta) \tag{14}$$

In (12), the terms with coefficients $K_2, K_3, K_4, K_6, K_8, K_{10}, K_{13}$ can be replaced with $V^2_{0,\theta}\cos^2(\beta)$, and the terms with the $\sin^2(\beta)$ in (12) can be substituted by an expression extracted from (13). Also, by noting that $\beta = 0°$ and $\theta = 0°$ in (12) yields $V^2_{0,0} = K_2 + K_4 + K_6 + K_{13}$ and by setting $m = K_{12} + K_{14} + K_{15} + K_{17}$, $n = K_9 + K_{11}$ and writing $\boldsymbol{\nu}_{\beta,\theta} \equiv V^2_{\beta,\theta}$, $\boldsymbol{\nu}_{0,\theta} \equiv V^2_{0,\theta}$ and $\boldsymbol{\nu}_{\beta,0} \equiv V^2_{\beta,0}$, the factorization and rearrangement of identical terms in (12) simplifies the expression for $V_{\beta,\theta}$ to

$$\boldsymbol{\nu}_{\beta,\Theta} = \boldsymbol{\nu}_{0,\theta}\cos^2(\beta) + \boldsymbol{\nu}_{\beta,0} - \boldsymbol{\nu}_{0,0}\cos^2(\beta) + \sin(\beta)\cos(\beta)\left\{m\left(\cos(\theta)-1\right) + n\sin(\theta)\right\} \tag{15}$$

Coefficients m and n in (15) can be evaluated analytically by considering the boundary conditions imposed on the sensor's operation. For instance, for a full operation range of $0 \le \beta \le 90°$, $0 \le \theta \le 90°$, the boundary condition $\boldsymbol{\nu}_{\beta,\theta}\big|_{\theta=90°} = 0$ generates the equation

$$\boldsymbol{\nu}_{\beta,0} - \boldsymbol{\nu}_{0,0}\cos^2(\beta) + \sin(\beta)\cos(\beta)\{n-m\} = 0 \tag{16}$$

and the boundary condition at the peak value of the voltage profile defined by the first derivative test $\left(\partial \boldsymbol{\nu}_{\beta,\theta} / \partial\theta\right)\big|_{\theta=0°} = 0$, generates the equation

$$\left\{\boldsymbol{\nu}'_{0,\theta}\cos^2(\beta) + \sin(\beta)\cos(\beta)\left[-m\sin(\theta) + n\cos(\theta)\right]\right\}\Big|_{\theta=0°} = 0 \tag{17}$$

where $\boldsymbol{\nu}'_{0,\theta}$ denotes the first derivative of $\boldsymbol{\nu}_{0,\theta}$. Using (16) and (17), a simultaneous system of two equations with two unknowns can be resolved to yield two analytical expressions for *m* and *n*, which upon substitution in (15), generate the final expression for the self-calibrating model of the piezoelectric tilt sensor in Fig. 1 as

$$\boldsymbol{\nu}_{\beta,\theta} = \boldsymbol{\nu}_{0,\theta}\cos^2(\beta) + \boldsymbol{\nu}_{\beta,0} - \boldsymbol{\nu}_{0,0}\cos^2(\beta) + (\cos(\theta)-1)\left\{\boldsymbol{\nu}_{\beta,0} - (\boldsymbol{\nu}'_{0,\theta}\big|_{\theta=0°} + \boldsymbol{\nu}_{0,0})\cos^2(\beta)\right\} - \boldsymbol{\nu}'_{0,\theta}\big|_{\theta=0°}\sin(\theta)\cos^2(\beta) \tag{18}$$

We note that this model represents a trigonometric function of β and θ, and the genetic data $\boldsymbol{\nu}_{\beta,0}$, $\boldsymbol{\nu}_{0,\theta}$ and $\boldsymbol{\nu}_{0,0}$, only.

4. SIMULATION RESULTS

Three simulation results are carried on a CAD model of the tilt sensor shown in Fig. 1 under variable temperature conditions shown separately in Figs. 3, 4 and 5. For the same dimensions of the sensor, the voltage output of the PZT layer varies as a function of temperature. However, since the self-calibrating model derived in (18) does not explicitly depend on temperature, the tuning of the model to account for these thermal variations is performed via re-calibration and re-generation of the genetic data $\boldsymbol{\nu}_{\beta,0}$, $\boldsymbol{\nu}_{0,\theta}$ and $\boldsymbol{\nu}_{0,0}$, only.

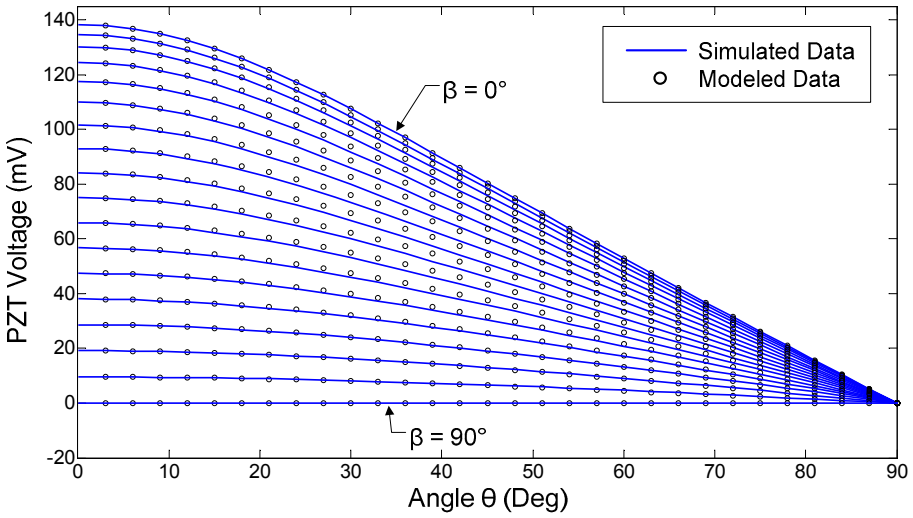

Figure 3. Simulated and modeled data for the PZT voltage output at temperature **288°**K for $\beta = 0:5:90°$ and $0 \le \theta \le 90°$

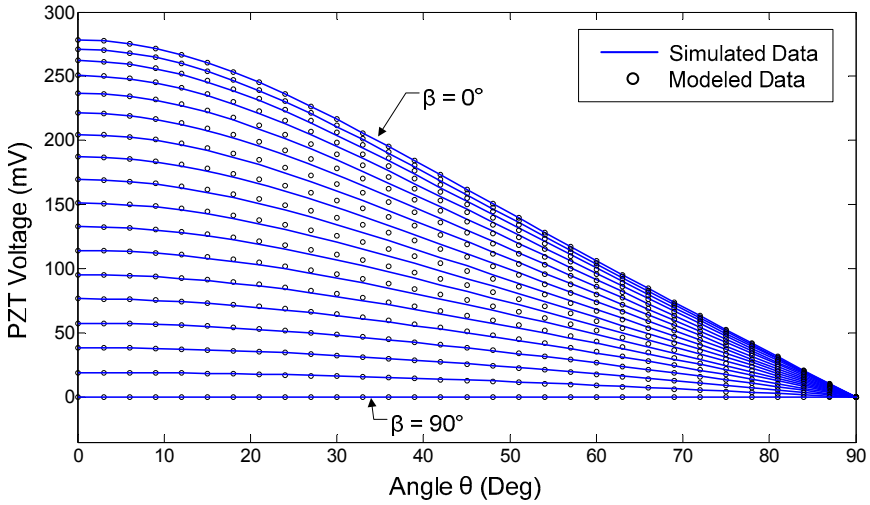

Figure 4. Simulated and modeled data for the PZT voltage output at temperature **303°**K for $\beta = 0:5:90°$ and $0 \le \theta \le 90°$

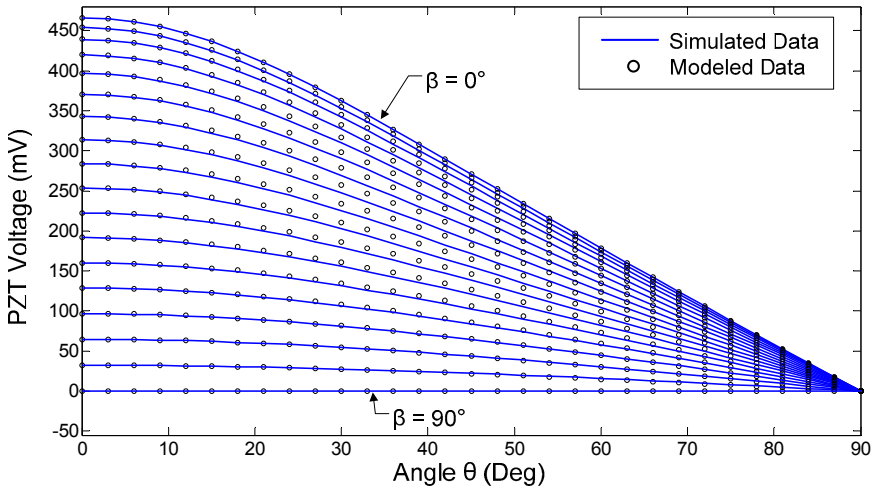

Figure 5. Simulated and modeled data for the PZT voltage output at temperature **323°**K for $\beta = 0:5:90°$ and $0 \le \theta \le 90°$

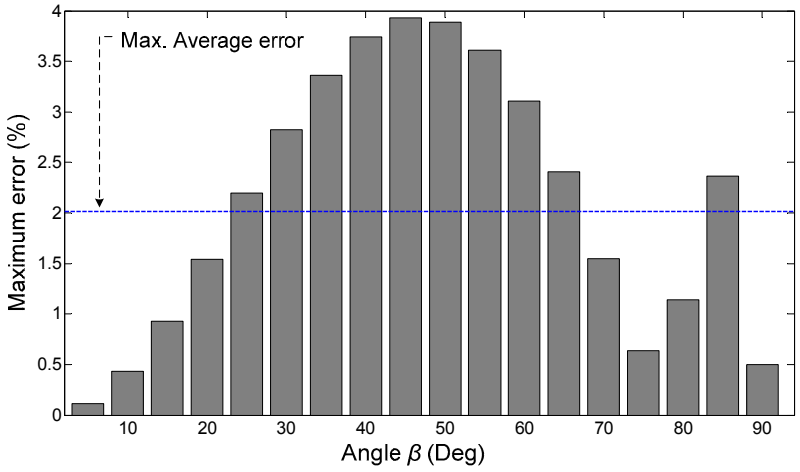

Figure 6. Maximum percent error offset (%) between modeled and simulated data as a function of $0 \le \beta \le 90°$

The accuracy of the model in (18) is highlighted by cross-comparing the modeled data to the simulation data generated on CoventorWare. This cross-comparison is plotted in Fig. 3 for an operating temperature of 288°K, in Fig. 4 for a temperature of 303°K, and in Fig. 5 for a temperature of 323°K. Although all profiles in these simulations meet the boundary conditions, the offset between the modeled and simulated data tends to vary as a function of angle β. This variation is depicted in Fig. 6, where the *maximum* percent error offset is plotted over the full roll range of $0 \le \beta \le 90°$. Based on this chart, the maximum percent error remains under 4% over the entire β-range, with an average maximum error of 2.01% and a peak error of 3.92% occurring around the middle range.

5. CONCLUSION

In this paper, a self-calibrating model for a new MEMS piezo-electric dual-axis tilt sensor is presented. The derivation of the model shows that the resulting expression is independent of any geometric, structural, electro-mechanical or piezoelectric properties of the sensor and the PZT layer. This information is rather carried implicitly by genetic data generated through calibration. This makes the ensuing model impervious to variations in the operating conditions, such as temperature. This property, along with the accuracy of the self-calibrating model, were demonstrated through three case-study simulations with variable 288°K, 303°K and 323°K temperature conditions. Future work will investigate the generalizable aspect of the proposed self-calibrating modeling technique.

REFERENCES

[1] Akiyama, M., Morofuji, Y., Kamohara, T., Nishikubo, K., Tsubai, M., Fukuda, O., and Ueno, N., "Flexible Piezoelectric Pressure Sensors Using Oriented Aluminum Nitride Thin Films Prepared on Polyethylene Terephthalate Films," J. Applied Physics, 100(11), 114318 – 114318-5 (2006).

[2] Zou, Q., Tan, W., Kim, E.S., and G.E. Loeb, "Single- and Triaxis Piezoelectric-Bimorph Accelerometers," J. Microelectromechanical Systems, 17(1), 45 – 57 (2008).

[3] Sabata, R.G., Mukherjee, B.K., Ren, W., and Yang, G., "Temperature Dependence of the Complete Material Coefficients Matrix of Soft and Hard Doped Piezoelectric Lead Zirconate Titanate Ceramics," J. Applied Physics, 101(6), 064111 – 064111-7 (2007).

[4] Ivira, B., Benech, P., Fillit, R., Ndagijimana, F., Ancey, P., and Parat, G., "Modeling for Temperature Compensation and Temperature Characterizations of BAW Resonators at GHz Frequencies," IEEE Transactions on Ultrasonics, Ferroelectrics, and Frequency Control, 55(2), 421 – 430 (2008).

[5] Feng, Z., and Rena, X., "Aging Effect and Large Recoverable Electrostrain in Mn-doped KNbO3-based ferroelectrics," J. Applied Physics Letters, 91(3), 032904 – 032904-3 (2007).

[6] Xu, G., Wang, X., Yang, D., Duan, Z., Feng, C., and Chen, K., "Peculiar Temperature Aging Effects on the Piezoelectric Constant of $Pb(Mg_{1/3}Nb_{2/3})O_3$-$PbTiO_3$ Single Crystal Near the Morphotropic Phase Boundary," J. Applied Physics Letters, 86(3), 032902 – 032902-3 (2005).

[7] Wonga, C.K., Poon Y.M., and Shin, F.G., "Temperature Dependence of the Complex Effective Piezoelectric Coefficient of Ferroelectric 0-3 Composites," J. Applied Physics, 92(6), 3287 – 3287-6 (2002).

[8] Priya, S., Ryu, J., Uchino, K., and Viehland, D., "Mechanical Aging Behavior of Oriented $Pb(Mg_{1/3}Nb_{2/3})O_3$–$PbTiO_3$ and $Pb(Zn_{1/3}Nb_{2/3})O_3$–$PbTiO_3$ Single Crystals,", J. Applied Physics Letters, 79(16), 2624 – 2624-3 (2001).

[9] Zhang, H., Jiang, S., Xiao, J., and Kajiyoshi, K., "Piezoelectric and Dielectric Aging of $Bi_{0.5}(Na_{0.82}K_{0.18})_{0.5}TiO_3$ Lead-free Ferroelectric Thick Films," J. Applied Physics, 107(12), 124118 – 124118-6 (2010).

[10] Kugela, V.D., and Cross, L.E., "Behavior of soft piezoelectric ceramics under high sinusoidal electric fields," J. Applied Physics, 84(5), 2815 – 2815-16 (1998).

[11] Chen, Q., Zhang, T., and Wang, Q-M., "Frequency-temperature Compensation of Piezoelectric Resonators by Electric DC Bias Field," IEEE Transactions on Ultrasonics, Ferroelectrics, and Frequency Control, 52(10), 1627 – 1631 (2005).

[12] Quagliarella, L., Sasanelli, N., and Monaco, V., "Drift in Posturography Systems Equipped With a Piezoelectric Force Platform: Analysis and Numerical Compensation," IEEE Transactions on Instrumentation and Measurement, 57(5), 997 – 1004 (2008).

[13] Moubarak, P.M., Ben-Tzvi, P., and Zaghloul, M.E., "A Self-Calibrating Mathematical Model of the Direct Piezoelectric Effect of a New MEMS Tilt Sensor," IEEE Sensors Journal, doi: 10.1109/JSEN.2011.2173188, Available Online: http://ieeexplore.ieee.org/stamp/stamp.jsp?tp=&arnumber=6058573&isnumber=4427201, 2011.